Understanding the dynamic perturbative behaviour of Electrolyte-Gated FET based Biosensors with Immobilised Nanoparticles

Naveen Kumar
DeepNano Group, James Watt School of Engineering, University of Glasgow
Glasgow, United Kingdom
naveen.kumar@glasgow.ac.uk

César Pascual García
Materials Research and Technology Department, Luxembourg Institute of Science and Technology
Belvaux, Luxembourg
cesar.pascual@list.lu

Ankit Dixit
DeepNano Group, James Watt School of Engineering, University of Glasgow
Glasgow, United Kingdom
ankit.dixit@glasgow.ac.uk

Vihar Georgiev
DeepNano Group, James Watt School of Engineering, University of Glasgow
Glasgow, United Kingdom
vihar.georgiev@glasgow.ac.uk

2024 International Conference on Simulation of Semiconductor Processes and Devices (SISPAD) | 979-8-3315-1635-2/24/$31.00 ©2024 IEEE | DOI: 10.1109/SISPAD62626.2024.10733212

***Abstract*— In this study, we introduce a novel methodology to investigate and model the nonlinear perturbative behaviour in an Electrolyte-Gated Field-Effect Transistor (EGFET) based on biosensors that are enhanced with immobilised nanoparticles. Our approach systematically addresses the perturbations occurring due to redundant silanol sites by quantifying their impact on sensor output, thereby improving the reliability of the sensor readings. Additionally, we explore the role of neutral gold nanoparticles in augmenting the sensor ability to detect and differentiate amino acid fingerprints effectively. Moreover, our research delves into the effects of random partial hybridisation of carboxylic acids (amino acids) under varying conditions, which alter the reactive sites available for binding. By integrating these factors into our analysis, we provide a robust framework for calibrating and benchmarking experimental data.**

Keywords—Electrolyte-Gated FET, Biosensor, Nanoparticles, Non-Linearity, Gold Nanoparticles, Silanol Sites, tert-butyloxycarbonyl (BOC), APTES, Protective Group

I. Introduction

In the evolving landscape of biosensing technologies, Electrolyte-Gated Field-Effect Transistors (EG-FETs) [1] represent a significant leap forward, particularly when integrated with nanoparticle-modified surfaces [2][3][4]. EG-FETs, by design, leverage the field-effect modulation of charge carriers near the sensor surface to transduce biological interactions into measurable electrical signals [5][6]. The presence of an electrolyte as the gating medium introduces a spectrum of non-linearities, primarily due to the dual ionic-electronic conduction mechanisms [7]. These non-linearities, often manifesting as shifts in threshold voltage or changes in the transconductance, are significantly influenced by the interaction of biological analytes with the sensor surface. Further complicating this response are the silanol sites [8] on the sensor surface, which can interact with the electrolyte ions, altering the local charge environment and, consequently, the sensor output.

The integration of nanoparticles (NPs) onto the biosensing surface introduces additional variables into this already complex system. NPs can enhance the effective surface area and promote higher degrees of biomolecular interactions due to their high surface-to-volume ratio [9]. This manuscript explores how different nanoparticles, particularly those immobilised via silane coupling agents such as (3-Aminopropyl)triethoxysilane (APTES), affect the biosensor performance [10][11]. The effect of capping these nanoparticles with various protective groups to shield the amine sites on APTES from non-specific interactions is analysed in detail. These protective strategies are vital for minimising false signals and enhancing the robustness and reliability of the biosensor under test conditions.

Through analytical modeling, this research endeavours to provide a comprehensive understanding of how these multiple layers of complexity interact within an EG-FET biosensor. The insights gained not only contribute to the fundamental science of biosensor materials but also pave the way for the design of the next-generation biosensors with enhanced analytical performance for real-world biological and chemical sensing applications.

II. Methodology

The proposed architecture to capture the perturbations is derived from the solution of the Gouy-Chapman-Stern and Site-Binding model simultaneously providing the effective surface potential due to the amino acids [12][13]. The silanol sites act as separate reactive sites in addition to the amino acids resulting in a superimposed surface potential from various components of distinct charge densities. The distinct charge densities, that occur due to amino acids, silanol sites or any non-specific bindings, are locally distributed but under electrolyte (highly conductive) these charge densities can be averaged over the sensing surface.

The amino acids with no sidechain, carboxylic side chain or amine sidechain immobilised along the carboxylic terminal can be represented by charge density σ_{o1}, σ_{o2}, and σ_{o3} respectively.

$$\sigma_{o1} = qN_S\left(\frac{cH_S}{cH_S + K_a}\right) \quad \textbf{(1)} \qquad \sigma_{o2} = qN_S\left(\frac{cH_S^2 - K_aK_b}{cH_S^2 + cH_S\,K_a + K_aK_b}\right) \quad \textbf{(2)}$$

$$\sigma_{o3} = qN_S\left(\frac{cH_S^2 + cH_S\,K_a}{cH_S^2 + cH_S\,K_a + K_aK_b}\right) \quad \textbf{(3)}$$

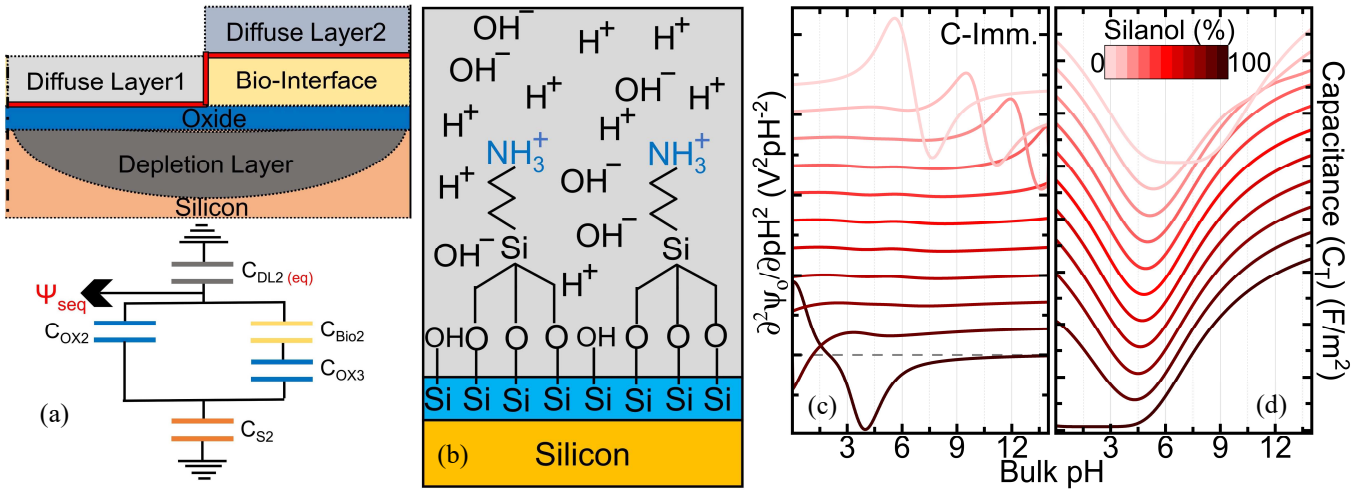

Figure 1. (a) Conceptual schematic view of the Electrolyte-gated Field Effect Transistors (EG-FETs) with subsequent boundaries of redundant silanol sites and biomolecule interface (Linker or amino acids) along with the capacitance circuit representing the shown layers (b) Approximated macroscopic view of EG-FET sensing surface with immobilised APTES and the electrolyte interaction (c) 2nd order derivative of surface potential (d) Total capacitance corresponding to the bulk pH for different percentage of the redundant silanol reactive sites [Note: Fig. 1(c) and 1(d) are shifted vertically to show the zero-crossover points of the 2nd order derivative of surface potential and Total capacitance]

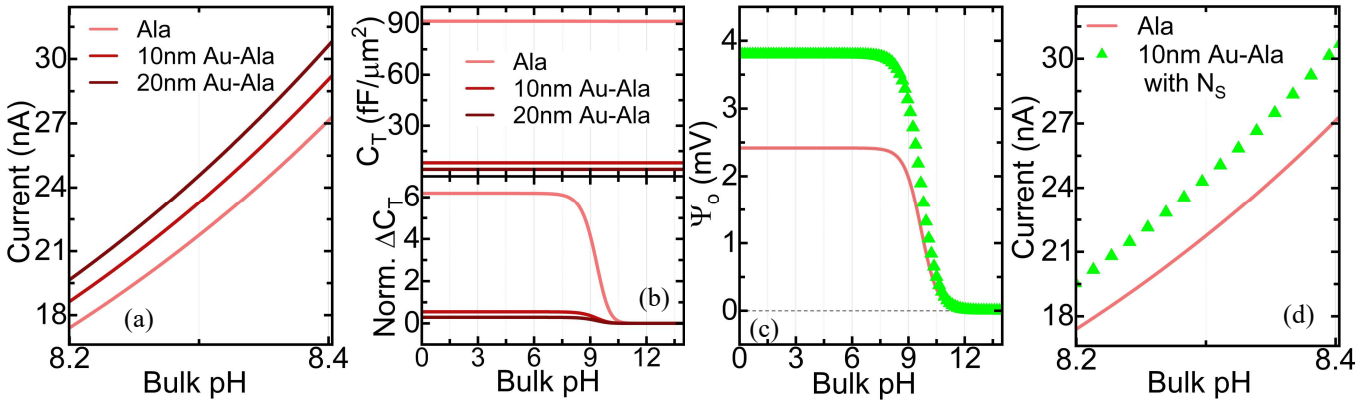

Figure 2. (a) Drain current (b) Total capacitance and normalised capacitance for Alanine (amino acid) on the sensing surface, Alanine with 10nm and 20nm diameter neutral gold nanoparticles relating to the bulk pH [Note: Amino acid density of the sensing surface with and without the nanoparticles is considered the same] (c) Surface potential (d) Drain current for Alanine (amino acid) on the sensing surface and Alanine with 10nm diameter neutral gold nanoparticles relating to the bulk pH [Note: Amino acid density of the sensing surface with and without the nanoparticles is different]

If we consider the presence of redundant silanol sites, the total charge density will be the summation of the respective charge density of amino acid and σ_{o2} with the dissociation constants of silanol sites.

III. Results And Discussion

Here, we have studied the case of Carboxyl-terminal immobilised aspartic acid (D) having an amine and carboxylic sidechain with SiO_2 as a gate oxide for the FET [Fig. 1(a)] [3]. The total surface states (N_T) are composed of attached analytes (AA) (N_{AA}) and the free silanol sites ($N_{OH} = N_T - N_{AA}$) that contribute to the surface charge density (σ_0) [Fig. 1(b)]. The presence of silanol sites changes the surface potential and isoelectric point due to the superposition of charge from the protonated/deprotonated silanol radicals with the AA depending on the pH value. The silanol site is more prone to acquire a negative charge as compared to the carboxylic radical of D but silanol site is less effective in protonating as compared to the amine radical of D. As the percentage of the silanol sites increases from a low value (0%) to 10%, the surface potential tends to have lower values due to a more acidic dissociation constant of silanol sites as compared to the carboxyl sites of aspartic acid [Fig. 1(c)]. The zero-crossover point of the double gradient correlates with the isoelectric point of the system with either 100% AA or silanol sites. The isoelectric point shifts to acidic values as the percentage of the silanol sites keeps increasing due to the higher effect of smaller dissociation constants of silanol radicals. In the presence of reactive sites from AA and silanol, the zero-crossover point depicts the change in the slope of surface potential and the ascendancy of the silanol over the AAs. At lower silanol contributions, D dominates the behaviour in $d^2\Psi_o/dpH^2$, which is more significant in the range of alkaline pH values as compared to the acidic range due to the early deprotonation of silanol radicals. As the isoelectric point shifts to more acidic values, the maxima of $d^2\Psi_o/dpH^2$ associated with the amino groups however shift to the right to leave space for changes in convexity that occur because of the contributions from the silanol groups to the

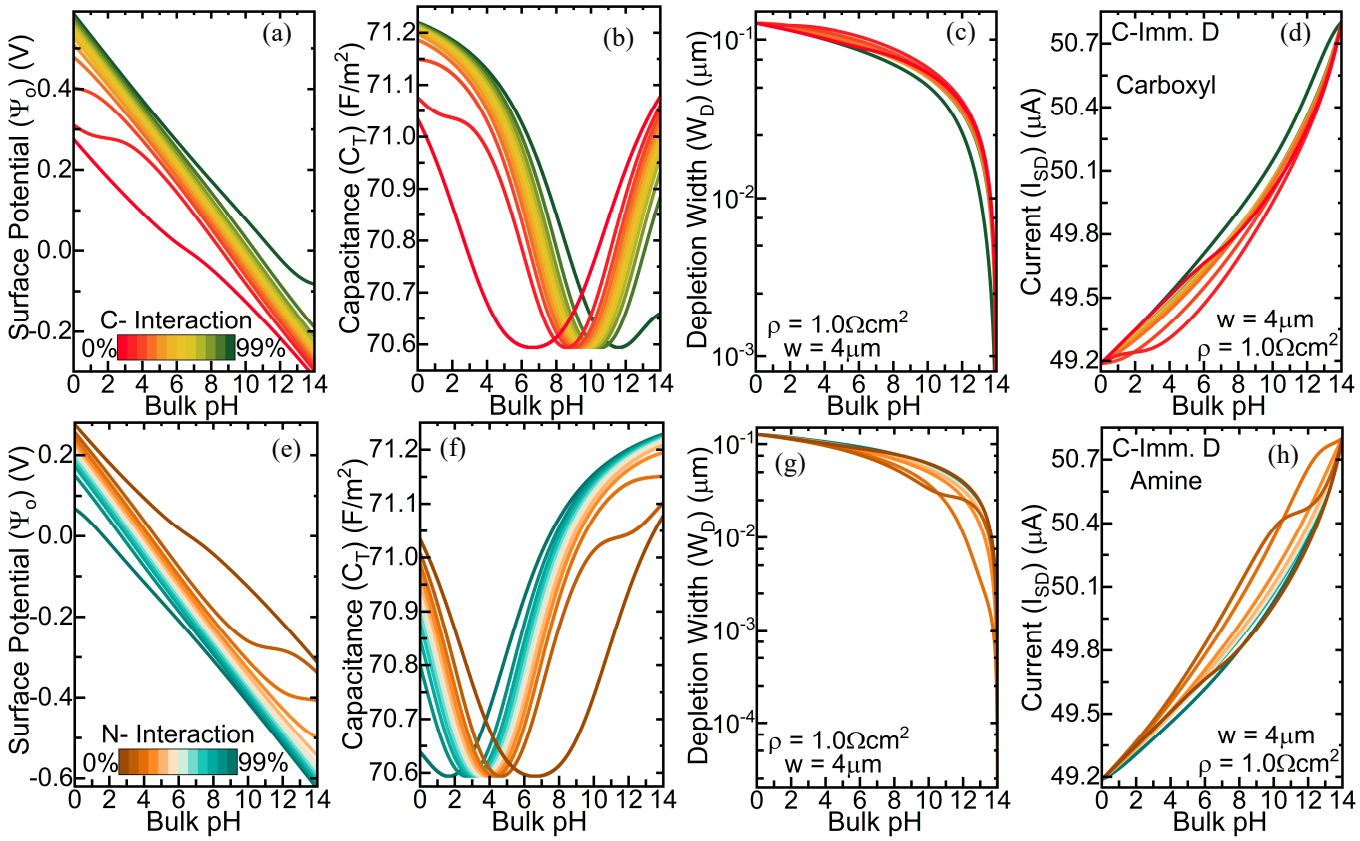

Figure 3. (a)/(e) Surface Potential (b)/(f) Total capacitance (c)/(g) Depletion width and (d)/(h) Current for C-terminal immobilised Carboxylic acid (D) on the sensing surface having different % of interactions with carboxylic/amine sidechain relating to the bulk pH respectively. [Note: The considered device is a Junctionless p-type FET with the resistivity of 1Ωcm^{-2}, width of 4μm and channel length = 10μm; The considered surface state density for the amino acid interactions is 5x10^{14}cm^{-2}]

electrostatic equilibrium with the double layer capacitance as shown in Fig. 1(d). Because of these contributions, the linearity of the surface potential increases flattening $d^2\Psi_o/dpH^2$, making precisely the most linear contribution at 50% contribution from each of the reactive sites. In the presence of a high contribution of silanol sites that decreases the effective affinity of the surface for protonation as compared to the individual amine sites of D, the behaviour is dominated by the silanol groups and the peaks of $d^2\Psi_o/dpH^2$ are then observed in the acidic range of pH.

For the enhancement of the amino acid fingerprints, we have considered the uniform density of the gold nanoparticles as a neutral sensing surface. Considering the equal density of amino acids on the sensing surface with and without the nanoparticles, the surface potential remains unchanged due to the same number of reactive sites. However, with the variation in nanoparticle size, there is a significant variation in the sensor capacitance and output signal as a drain current [Fig. 2(a) and 2(b)] due to an increase in the distance of the diffuse layer away from the oxide surface. As the nanoparticle size increases, the drain current increases as the considered device is p-type, which requires a higher bias to be turned off. Thus, as shown in Fig. 2(b), the decrease in effective oxide capacitance (including the nanoparticle capacitance) with the increase in nanoparticle size reduces the channel control allowing more current to flow across the device. The variation of the total capacitance as a function of the pH is higher for the amino acid in the absence of nanoparticles and it decreases with the increase in the size of nanoparticles due to the higher capacitance of nanoparticles as compared to the electrical double-layer capacitance. For different nanoparticle sizes, if the active surface area of nanoparticles is considered which is approx. 0.5π times larger than the total surface area without nanoparticles, there is a notable variation in the surface potential and the drain current of the biosensor as shown in Fig. 2(c) and 2(d).

We have also considered the different interactions of the carboxylic and amine-reactive sites of the Carboxyl-terminal immobilised carboxylic acid to capture the possible partial hybridisation of the amino acids as shown in Fig. 3. Assuming C-Imm. Aspartic acid (D) as an example, we have only two free reactive sites, one is the alpha-amine site and the other is the carboxyl sidechain. D is a trifunctional AA that after the immobilisation by the C-terminal remains with a free amine radical (pK = 9.60) and a sidechain of the carboxylic group (pK = 3.65). D acquires a positive charge at lower pH values due to the protonated amine and neutral carboxylic group. With an increase in pH, Ψ_o decreases from positive to negative values due to the deprotonation of the amine and carboxylic radicals changing the overall charge of the molecule and allowing the AA to have an isoelectric point in the zwitterion state, which happens at the pH value that is the average of the pK values of amine and carboxylic radicals. Using such a concept, our simulations showed that as the percentage of interactions with carboxylic sidechain increases from 0% to 99%, the surface potential decreases by approx. +0.25V at the highest acidity and

-0.2V at the highest alkalinity as shown in Fig. 3(a). As the interactions change the number of total reactive sites, the isoelectric point changes for the system. The total capacitance curve shifts to the higher alkaline pH with the increase in the interactions but the capacitance minima remain at the same value as shown in Fig. 3(b). The depletion width and the drain current follow the surface potential with the same range of variations as shown in Fig. 3(d) and 3(e). However, the variation of drain current realting to the Bulk pH mimics the significant change in surface potential keeping the zero-crossover point of 2nd order differentiation of drain current exactly as the isoelectric point or the pH at capacitance minima. The opposite trend can be observed with the interactions that happen with the amine site rather than the carboxylic sidechain as interactions with the amine site decrease the reactive sites that can acquire positive charges on the sensing surface as shown in Fig. 3(e). The capacitance curve shifts to the left with the increase in the amine interactions [Fig. 3(f)]. The depletion width and the current follow a similar pattern as that of the surface potential and total capacitance for different amine interactions as shown in Fig. 3(g) and Fig. 3(h) respectively. The proposed work can be helpful in detailing the non-linearities in the biosensors allowing better calibration and benchmarking of the experimental data.

IV. Conclusion

We have proposed a novel methodology to analyse the dynamic perturbation in the electrolyte-gated FET based biosensors due to the redundant silanol sites, partial-hybridisation of the amino acids reactive sites and captured the effect of nanoparticles on the sensitivity of the amino acids. The proposed model accounts for the effect of different sizes of nanoparticles along with the amino acid density variation in the sensing surface. The zero-crossover fingerprints of the 2nd order differentiation of surface potential and capacitance minima variation relating to the pH help in quantifying the effect of redundant silanol sites. The interactions with the carboxylic and amine terminals of the amino acids provide significant information about the binding sites for protein-peptide interactions. The optimised analytical module paves the way for an accurate and reliable protein sequencing tool.

Acknowledgment

This work received funding from the European Innovation Council under the Horizon 2020 program of Future Emerging Technologies. Project: 862539 — ElectroMed and from the Luxembourg National Research Fund (FNR) under the project C22/MS/17380687/PROFET-SEQ.

References

[1]. Wang, G.Y., Lian, K. and Chu, T.Y., 2021. Electrolyte-gated field effect transistors in biological sensing: a survey of electrolytes. IEEE Journal of the Electron Devices Society, 9, pp.939-950.

[2]. Neubert, T.J., Krieg, J., Yadav, A. and Balasubramanian, K., 2022. PH sensitivity of edge-gated graphene field-effect devices with covalent edge functionalization. ACS Applied Electronic Materials, 4(9), pp.4668-4676.

[3]. Singh, K., Lou, B.S., Her, J.L., Pang, S.T. and Pan, T.M., 2019. Super Nernstian pH response and enzyme-free detection of glucose using sol-gel derived RuOx on PET flexible-based extended-gate field-effect transistor. Sensors and Actuators B: Chemical, 298, p.126837.

[4]. Liu, G., Luais, E. and Gooding, J.J., 2011. The fabrication of stable gold nanoparticle-modified interfaces for electrochemistry. Langmuir, 27(7), pp.4176-4183.

[5]. Bergveld, P., 1981. The operation of an ISFET as an electronic device. Sensors and Actuators, 1, pp.17-29.

[6]. Shojaei Baghini, M., Vilouras, A., Douthwaite, M., Georgiou, P. and Dahiya, R., 2022. Ultra‐thin ISFET‐based sensing systems. Electrochemical Science Advances, 2(6), p.e2100202.

[7]. Li, M., Pan, H., Liu, T., Xiong, X., Yu, X., Hu, Y.S., Li, H., Huang, X., Suo, L. and Chen, L., 2022. All-in-One Ionic–Electronic Dual-Carrier Conducting Framework Thickening All-Solid-State Electrode. ACS Energy Letters, 7(2), pp.766-772.

[8]. Woias, P., Meixner, L. and Fröstl, P., 1998. Slow pH response effects of silicon nitride ISFET sensors. Sensors and Actuators B: Chemical, 48(1-3), pp.501-504.

[9]. Luo, X.L., Xu, J.J., Zhao, W. and Chen, H.Y., 2004. Glucose biosensor based on ENFET doped with SiO2 nanoparticles. Sensors and Actuators B: Chemical, 97(2-3), pp.249-255.

[10]. Rani, D., Rollo, S., Olthuis, W., Krishnamoorthy, S. and Pascual García, C., 2021. Combining chemical functionalization and FinFET geometry for field effect sensors as accessible technology to optimize pH sensing. Chemosensors, 9(2), p.20.

[11]. Shukla, R.P., Bomer, J.G., Wijnperle, D., Kumar, N., Georgiev, V.P., Singh, A.C., Krishnamoorthy, S., Pascual García, C., Pud, S. and Olthuis, W., 2022. Planar junctionless field-effect transistor for detecting biomolecular interactions. Sensors, 22(15), p.5783.

[12]. Allagui, A., Benaoum, H. and Olendski, O., 2021. On the Gouy–Chapman–Stern model of the electrical double-layer structure with a generalized Boltzmann factor. Physica A: Statistical Mechanics and its Applications, 582, p.126252.

[13]. Kumar, N., García, C.P., Dixit, A., Rezaei, A. and Georgiev, V., 2023. Charge dynamics of amino acids fingerprints and the effect of density on FinFET-based Electrolyte-gated sensor. Solid-State Electronics, 210, p.108789.